Journal of Physics: Conference Series **663** (2015) 012003 doi:10.1088/1742-6596/663/1/012003

Morin transition in Hematite nanoparticles analyzed by neutron diffraction

J. I. Pérez-Landazábal[1*], C. Gómez-Polo[1], V. Recarte[1], S. Larumbe[1], V. Sánchez-Alarcos[1], M. Fernandes Silva[2], E.A Gómez Pineda[2], A.A. Winkler Hechenleitner[2], M.K. Lima[2] and J.A. Rodriguez-Velamazán[3,4]

[1]Departamento de Física, Universidad Pública de Navarra, Campus de Arrosadía 31006 Pamplona, Spain.

[2]Departamento de Química, Universidade Estadual de Maringá, 87020-900 Maringá-PR, Brazil

[3]Instituto de Ciencia de Materiales de Aragón, CSIC - Universidad de Zaragoza, Zaragoza, Spain

[4]Institut Laue-Langevin, CRG's D1B, F-38042 Grenoble, France

*E-mail: ipzlanda@unavarra.es

Abstract. Hematite (α-Fe_2O_3) undergoes a first order spin reorientation transition called the Morin transition: upon cooling, the moments align antiferromagnetically along the rhombohedral axis, and the net magnetic moment goes to zero. Morin transition temperature is around to 260K in bulk materials and depends on the mean particle size. In this work, the Morin transition has been studied by neutron diffraction as function of temperature and applied magnetic field in 47 nm nanoparticles. The Rietveld analysis of the diffraction spectra around the Morin transition shows a similar behavior to that found in bulk samples. On the other side, the magnetic field induced phase transformation has been analyzed.

1. Introduction

Because of their inherent environment-friendly feature, iron oxide materials have been extensively studied in diverse fields including catalysis [1,2], environment protection [3], gas sensors [4,5] magnetic storage media [6], and clinical diagnosis and treatment [7]. In order to pursue an excellent performance, many efforts have also been carried out on the synthesis and properties of iron oxide nanostructures [1,4,8,9]. Iron oxide is an important transition metal oxide which usually exists in nature in three phases: magnetite (Fe_3O_4), maghemite (γ-Fe_2O_3) and hematite (α-Fe_2O_3). Hematite is the most stable form of iron oxide (α-Fe_2O_3). Its electronic, catalytic and magnetic properties are of increasing interest from the application point of view in different fields [10]. At room temperature, hematite is weakly ferromagnetic with a rhombohedral corundum structure (Space group R-3c) [11]. The magnetic moments are approximately perpendicular to the rhombohedral axis with a small canting of the magnetic sublattices, giving a small net magnetic moment. Upon cooling, the material undergoes a first order spin reorientation transition, the Morin transition. The moments align antiferromagnetically along the rhombohedral axis and the net magnetic moment goes to zero. Morin transition temperature T_m, is around to 260 K in bulk materials [12,13]. However, T_m depends on the mean particle size, d. When the size is smaller than 100 nm, T_m decreases abruptly [14,15]. This effect is due to the increase of the surface-volume ratio of the particles, which yields to a lack of symmetry at

nanometric scale. Therefore, particle size reduction hinders the magnetic interaction producing the long-range antiferromagnetic order. For nanoparticles smaller than 10 nm, the antiferromagnetic order does completely vanish [16]. In this work, the Morin transition has been studied by neutron diffraction as function of temperature and applied magnetic field. The Rietveld analysis of the diffraction spectra around the Morin transition shows a similar behavior to that found in bulk samples. On the other side, the magnetic field induced phase transformation has been analyzed "In situ" in the diffractometer.

2. Experimental

Nanoparticles of hematite were elaborated by modified aqueous sol-gel method [17]. Saturated aqueous metal nitrate solution was prepared and maintained at room temperature under stirring for two hours. After that, it is heated under vigorous stirring until total water evaporation. The temperature was maintained at 250 ºC until the total thermal degradation. The nanostructured material was obtained after burning the precursor powder under air atmosphere at 400 ºC. The mean diameter size is 47 nm determined by Scherrer formula after instrumental correction but particles show irregular shapes. Neutron diffraction experiments were performed on the D1B (CRG-D1B-12-249). The Rietveld Method as implemented in the the Fullprof [18] program has been used to analyze the neutron spectra.

3. Results and Discussions

Figure 1 shows a three-dimensional picture (intensity, angle 2θ and temperature) of the phase evolution observed "in situ" at the diffractometer. At room temperature, the diffraction pattern corresponds to hematite (Space group R-3c). The transition to the antiferromagnetic structure can be detected at around T_m=240K through the pure magnetic (003) reflection measured at 32º (rhombohedral setting). The peak intensity linked to the ferromagnetic phase lowers as the temperature decreases. Results show the absence of changes in the transformation temperature when compared with bulk alloys. On the other side, a multidomain structure is expected to be present due to the particle size and then interparticle interaction could be neglected [19].

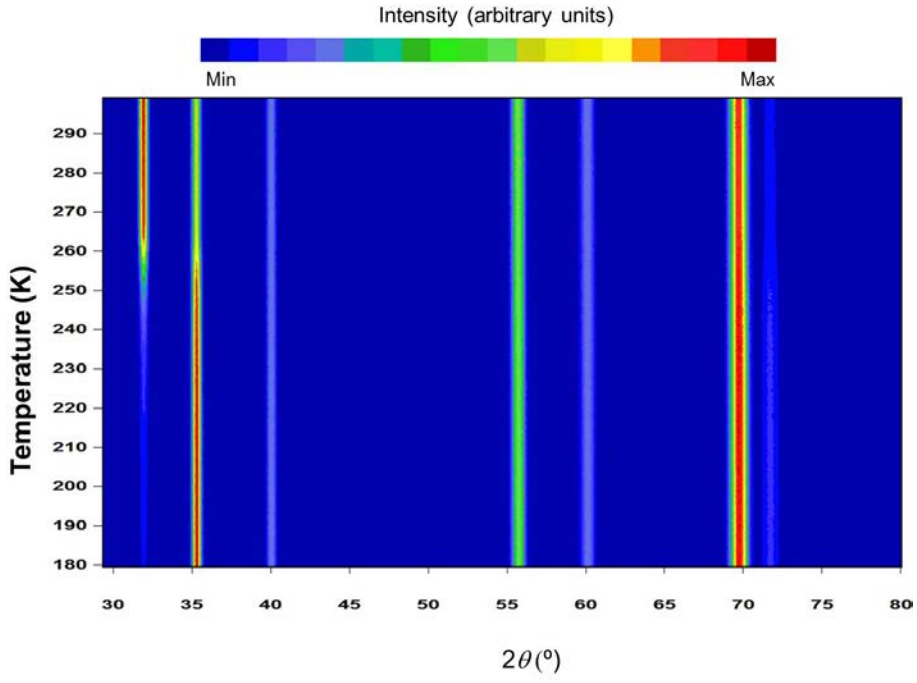

Figure 1: Thermo-diffraction patterns in a mesh-plot corresponding to the hematite nanoparticles of 47 nm size. The colour code indicates different intensities (in arbitrary units) from blue (minimum) to red (maximum). The Morin transition is clearly noticed by an increase of the intensity of the reflection at 2θ *ca.* 32º and a decrease of the reflection at 2θ *ca.* 35º.

Figure 2 shows the observed and calculated neutron powder diffraction patterns from D1B for α-Fe_2O_3 at 280 K (above) and 200 K (below). The difference between observed and calculated is shown below the diffraction patterns, with tick marks indicating the Bragg reflection positions from the nuclear and magnetic contribution. The (003) Bragg reflection is also indicated.

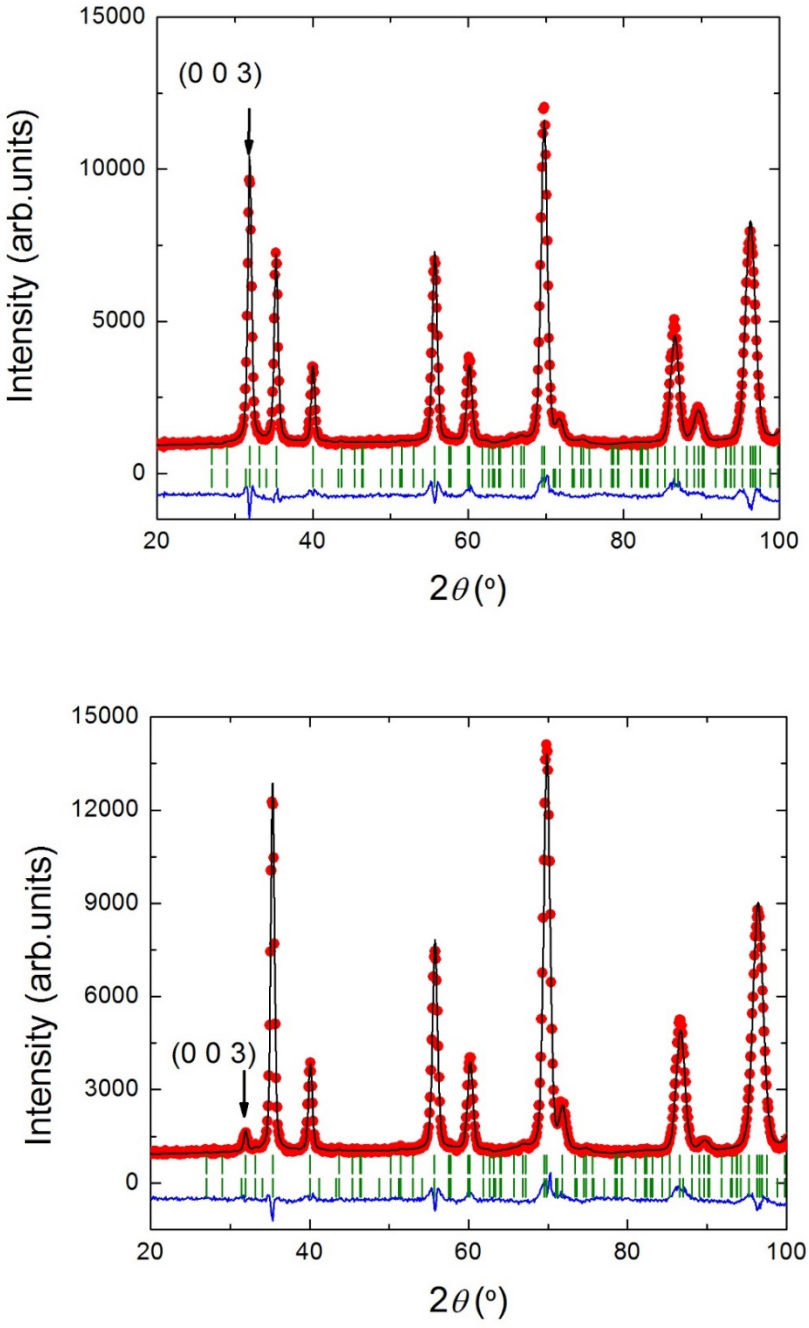

Figure 2: Refined patterns for T = 280 K ($T>T_M$)-Above and T = 200 K ($T<T_M$)-Below. The experimental data have been represented as red circles, the calculated curve as solid black line and the difference between them as solid blue line. The green vertical lines represent the Bragg positions for the nuclear (top) and magnetic (bottom) phases.

Crystallographic and magnetic information obtained at 10 K and 280 K are shown in Table 1. As the symmetry of the system does not allow to determine the direction of the magnetic moment in the hexagonal basal plane, we can only distinguish between the in-plane and out-plane components of the magnetic moment. Above T_m, the magnetic moments are approximately perpendicular to the rhombohedral axis with a small canting of the magnetic sublattices with the scattering plane (around 17º), giving a small net magnetic moment. Upon cooling below 250 K, the moments align antiferromagnetically along the rhombohedral axis and the net magnetic moment goes to nearly zero. This change is mainly reflected in the the intensity of the (003) peak changing radically to a much smaller value below T_m, (see figure 1) although at least six reflections have important magnetic contribution reducing the magnetic Bragg error.

	10 K	**270 K**
a (Å)	5.0254(1)	5.0298(1)
c (Å)	13.7215(6)	13.7372(8)
Magnetic moment on plane (μB)	0.869(35)	3.566(24)
Magnetic moment out of plane (μB)	3.840(22)	1.115(76)
R_{mag}(%)	7.91	6.62

Table 1: Refined cell parameters and in-plane and out of plane magnetic moments at 10 K (below T_m) and 270 K (above T_m).

Nevertheless, the moments are not perfectly aligned with the rhombohedral axis. The Rietveld refinement of the structure at low temperature gives an estimate of the angle at which the moments tilt out away from the [111] direction. This angle is around 12.6 º at 10 K, which agrees with previously published values [20,21].

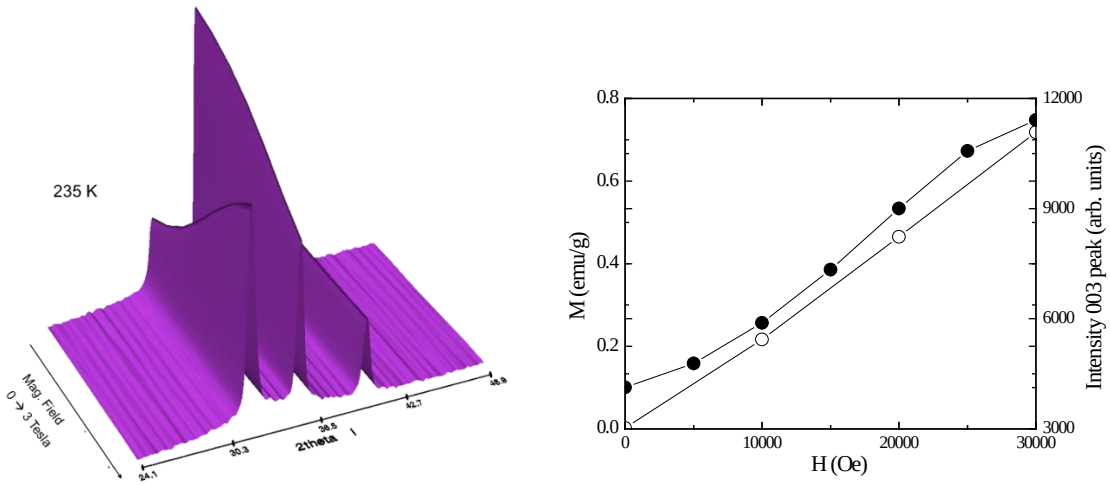

Figure 3: Magnetic field induced Morin transition recorded at 235 K (Left) and magnetization [22] and the (003) reflection intensity as a function of the applied magnetic field (Right).

Finally, regarding the magnetostructural transition, an increase in magnetization upon heating across the Morin transition has been observed previously [22]. The magnetization change during the transformation has been estimated as $\Delta M=0.3$ emu/g for the maximum applied field of H=60 kOe. Besides, a shift of the Morin transition to lower temperatures as the applied magnetic field increases, indicates that the magnetic field stabilizes the high temperature phase with respect to the low temperature one. Thus, the Morin transition should be induced by an external magnetic field in a particular temperature range. Figure 3 (left) shows, for example, the effect of a magnetic field application at T= 235 K. The sample is in the antiferromagnetic state at zero field but the application of a 30 kOe leads to the weak ferromagnetic phase as shown by the large increase of the (003) reflection intensity. This direct observation evidences the magnetic field induced transition from anti to ferromagnetic behavior. Figure 3 (Right) shows a comparison between the magnetization measured by squid magnetometry [22] and the (003) reflection intensity as a function of the applied magnetic field.

4. Conclusions

Neutron diffraction experiments performed "*In Situ*" allow determining the magnetic transition that occurs in Hematite nanoparticles. The Rietveld analysis of the diffraction spectra around the Morin transition shows a similar behavior to that found in bulk samples. On the other side, the magnetic field induced phase transformation from anti to ferromagnetic state has been observed.

Acknowledgements

The Institute Laue-Langevin and SpINS are acknowledged for the allocated neutron beamtime (CRG-D1B-12-249). JARV acknowledges CSIC for a JAEdoc contract.

References

[1] Tsodikov M V, Rostovshchikova T N, Smimov V V, Kiseleva O I, Maksimov Y V, Suzdalev I P and Ikorskii V N 2005 *Catal. Today* **105** 634.
[2] Zheng Y H, Cheng Y, Wang Y S, Bao F, Zhou L H, Wei X F, Zhang Y Y and Zheng Q 2006 J. *Phys. Chem. B* **110** 3093.
[3] Zhong L S, Hu J S, Liang H P, Cao A M, Song and Wan L J 2006 *Adv. Mater.* **18** 2426.
[4] Yang Y,Ma H X,Zhuang J, and Wang X 2011*Inorg. Chem.* **50** 10143.
[5] Chen J, Xu L N, Li W Y and Gou X L 2005 *Adv. Mater.* **17** 582.
[6] Zeng H, Li J, Liu J P, Wang Z L and Sun S H 2002 *Nature* **420** 520.
[7] Gupta A K and Gupta M 2005 *Biomaterials* **26** 3995.
[8] Bronstein L M, Huang X L, Retrum J, Schmucker A, Pink M, Stein B D and Dragnea B 2007 *Chem. Mater.* **19** 3624.
[9] Herrera F, Lopez A, Mascolo G and Albers E, Kiwi J 2001 *Appl. Catal. B* **29** 147.
[10] Navrotsky A, Mazeina L and Majzlan J 2008 *Science* **319** 1635.
[11] Gupta R K, Ghosh K, Dong L and Kahol P K 2010*Mater. Lett.* **64** 2132.
[12] Bengoa J F, Alvarez A M, Bianchi A E, Punte G, Vandenberghe R E, Mercader R C and Marchetti S G 2010 *Mater. Chem. Phys.* **123** 191
[13] Zysler R D, Fioran Di. Testa A M, Suber L, Agostinelli E and Godinho M 2003*Phys. Rev. B* **68** 212408.
[14] Özdemir O, Dunlop D J, and Berquó T S 2008 *Geochemistry Geophysics Geosystems* **9** Q10Z01.
[15] Amin N and Arajs S 1985*Phys. Rev. B* **35** 4810.
[16] Bødker F and Mørup S 2000*Europhys. Lett.* **52** 217 .
[17] Fernandes D M, Winkler Hechenleitner A A, Lima S M, Andrade L H C, Caires A R L and Gómez Pineda E A 2011Mater. *Chem.Phys.* **128** 371.
[18] Rodriguez-Carvajal J 1993 *Physica B* **192** 55.

[19] Frandsen C, Lefmann K, Lebech B, Bahl C R H, Brok E, Ancoña S N, Theil Kuhn L, Keller L, Kasama T, Gontard L C and Morup S 2011 *Phys. Rev. B* **84** 214435
[20] Krén E, Molnàr B, Svàb E, Zsoldos E 1974 *Solid State Commun.* **15** 1707.
[21] Hill A H, Jiao F, Bruce P G, Harrison A, Kockelmann W and Ritter C 2008 *Chem. Mater.* **20** 4891.
[22] Pastor J M, Pérez-Landazábal J I, Gómez-Polo C, Recarte V, Larumbe S, Santamarta R, Fernandes Silva M, Gómez Pineda E A, Winkler Hechenleitner A A and Lima K M 2012 *Appl. Phys. Lett.* **100** 063102.